Simulation of hydraulic heterogeneity and upscaling permeability and dispersivity in sandy-clay formations[1]

by Veronika A. Bakshevskaia[1] and Sergey P. Pozdniakov[2]

[1]Water Environment Preservation Department, Water Problems Institute, Russian Academy of Sciences, Gubkin St., 3, 119333 Moscow, Russia; e-mail: bakshev@mail.ru

[2]Faculty of Geology, Moscow State University, Leninskiye Gory, GSP-1, 119991 Moscow, Russia; e-mail: sppozd@geol.msu.ru

Abstract Since 1963, radioactive waste has been injected in deep artesian aquifers of Cretaceous terrigenous deposits in western Siberia. It is well known that geologic heterogeneity strongly affects contaminant transport in unconsolidated formations. To predict the long-term migration of this radioactive waste the effective hydraulic and macrodispersion parameters are estimated by using a three-dimensional high-resolution hydraulic heterogeneity model. The heterogeneous model of the injection area is developed by applying transition probability geostatistics. This model is used to simulate local steady-state groundwater flow and advective transport, leading to numerical estimates of effective hydraulic conductivity and macrodispersion parameters. Mean seepage velocities and effective longitudinal macrodispersion are calculated from observed breakthrough curves for a conservative tracer. Results show that mean horizontal lengths exceed vertical lengths by a factor of more than 30. As a result, vertical effective hydraulic conductivity is two orders of magnitude less than the horizontal effective conductivity. Observed breakthrough curves exhibit long tails and appear to be non-Fickian. Estimated effective longitudinal macrodispersivity in the vertical direction is one order of magnitude less than that in the horizontal direction.

Under a Fickian framework, this implies that dispersion modeling for regional transport simulations requires an anisotropic-media dispersion model.

KEY WORDS**:** Hydrogeology, stochastic simulations, Markov chain, effective hydraulic conductivity, anisotropy, macrodispersion

1 Introduction

Since 1963, liquid radioactive waste has been injected in artesian aquifers of Cretaceous terrigenous deposits in western Siberia. A total of 40,000,000 m^3 of liquid waste has been injected into aquifers at depths of 300–400 m (Rybalchenko et al. 1998). The main environmental and human-safety issue posed by this disposal site concerns potential radionuclide migration into the Tom River and the public water supply well fields (Shestakov et al. 2002). Therefore, the current injection and monitoring program must be supported by a system of models that estimate the risks associated with potential contaminant migration from the injection areas. Future long-term subsurface waste migration is subject to intensive regional-scale flow and transport modeling (Glinskii et al. 2014; Rybalchenko et al. 1998; Shestakov et al. 2002). These models are based on a simplified layered aquifer–aquitard geospatial description of the natural heterogeneity of injection formation, whereas the detailed study of well cores shows significant internal heterogeneity in each layer. This heterogeneity must be taken into account in long-term predictions of waste migration in the post-injection period.

The complex three-dimensional subsurface architecture of an aquifer may result in a highly heterogeneous spatial distribution of hydrogeological parameter values in porous media. This will significantly influence subsurface fluid flow and solute migration (De Marsily et al. 2005; Dell'Arciprete et al. 2014; Engdahl and Weissmann 2010; Feehley et al. 2000; Fogg et al. 2000; Zheng and Gorelick 2003; Zinn and Harvey 2003). Quantifying and predicting contaminant transport in heterogeneous geological formations is the subject of much research (Berkowitz et al. 2002; de Marsily et al. 2005; Neuman and Tartakovsky 2009). Difficulties in measuring and describing such heterogeneous systems lead to considerable uncertainty about contaminant transport. High-resolution models of hydraulic heterogeneities

are a promising means of overcoming this problem. Such models enable the study of transport effects, such as the possibility of preferable flow pathways, uncertainty of breakthrough curves, and upscale flow and transport parameters (Dell'Arciprete et al. 2014; Engdahl et al. 2010; Fleckenstein and Fogg 2008; Fogg et al. 2000; Liu et al. 2004; Sun et al. 2008; Zhang et al. 2007; Zinn and Harvey 2003).

It is difficult to select the best model for predicting long-term, regional-scale waste transport at this site. This is because high-resolution three-dimensional models cannot be applied to regional-scale transport modeling, and so an upscaling method must be used to determine the parameters of a simplified model (Pozdniakov et al. 2003; Pozdniakov et al. 2005).

The goal of this paper is threefold: (i) to develop a formation heterogeneity model conditioned on well-log data; (ii) to estimate the effective hydraulic and macrodispersion parameters and their relation with the model parameters; and (iii) to examine the upscaling of hydraulic conductivity rules for a coarse grid.

The remainder of this paper is organized as follows. The next Sect. contains a site description and summarizes the results of previous studies. Section 3 describes the development of a three-dimensional model of heterogeneity. Section 4 describes a flow and transport simulation and effective parameter estimation methods. Section 5 describes the upscaling of hydraulic conductivity for a coarse grid, and Section 6 presents a summary of our work and draws together our conclusions.

2 Site Description and Hydrogeological Framework

The disposal site is located in the south-east of the West Siberian Artesian Basin, 15 km north of Seversk, on the right bank of the Tom River (Fig. 1). Most of the injected waste is low-level, unprocessed waste with a total activity ranging from 10^{-8} up to 10^{-6} Ci/L and total dissolved solids of about 10 g/L (Rybalchenko et al. 1998). Two well fields for Seversk's public water supply are located 10 to 13 km from the injection areas. The general direction of the flow is toward the regional discharge zone (i.e. the Tom River). The detailed hydrogeology of the disposal site and injection setting were described by Rybalchenko et al. (1998) and Foley et al. (1995). The layered geospatial model represents the vertical heterogeneity of the formation as a chain of seven aquifers, marked from bottom to top as I, II, III, IV, IVa, V, and VI (Fig.

2). These aquifers are separated by six semipermeable units, marked from bottom to top as A–F (Rybalchenko et al. 1998). Aquifers II and III are used for waste injection. Semipermeable layer D, which overlays aquifer III, is considered the main protection against vertical waste migration. The geological formation considered here includes the injection aquifers and the overlaying semipermeable layers that represent heterogeneous sand-clay strata formed in a continental near-sea border environment (Shestakov et al. 2002).

The current site operation plan states that injection will be terminated within the next few decades. Regional-scale flow and transport models for long-term waste migration forecast in groundwater are based on a simplified geospatial description of this natural heterogeneity of studied formation as layered system of permeable and semipermeable layers. With this conceptualization of the regional hydrogeology, in the post-injection period, the waste will spread laterally (because of natural advection toward the discharge area) within the permeable layers and vertically in the semipermeable layers. Thus, the liquid waste will be safely isolated from drinking water sources and environments for thousands of years (Shestakov et al. 2002).

Lithological studies of more than 200 wells show that each aquifer and semipermeable layer has a complex internal architecture consisting of successions of relatively high- and relatively low-permeability units. To take these into account in previous investigations, a three-dimensional flow and transport model of waste injection has been developed using a binary (sand-clay) hydraulic heterogeneity model of the site (Pozdniakov et al. 2005). As a result, the hydraulic heterogeneity model does not have the continuous semipermeable layers (such as layers C and D) used in regional flow models (Shestakov et al. 2002). The flow model was calibrated by modeling the injection cycle over one year. Data for the groundwater heads in monitoring wells were used to calibrate the hydraulic conductivities of both facies and elastic storage. The calibration results suggest that the horizontal hydraulic conductivity of sand is 0.86 m/day, the vertical hydraulic conductivity of sand is 0.009 m/day, and the isotropic hydraulic conductivity of clay facies is 4×10^{-5} m/day. The disadvantage of this approach to heterogeneity (Pozdniakov et al. 2005) is a simplification of the natural diversity of hydrofacies into a binary system. The high anisotropy of sand facies obtained during calibration is explained by using this simplification.

In addition, Pozdniakov et al. (2012) developed two models of heterogeneity by means of two geostatistical methods (transition probability/Markov chain (TP/MC) approach and a two-dimensional kriging interpolation of the thicknesses of elementary lithological layers). Simulations of conservative transport by particle tracking algorithms show that horizontal transport along layers is similar for both models. The results of a comparison show that the main differences between the models occur in the vertical flow and advective vertical transport of particles across the formation bedding. Taking the conservative nature of the kriging-based model into account, it is appropriate to use models based on the TP/MC method to analyze hypothetical accidents.

In view of the above, a three-dimensional high-resolution four-hydrofacies model of heterogeneity for the study site is developed.

3 Development of Three-Dimensional Model of Heterogeneity

Existing approaches to aquifer heterogeneity characterization and modeling include descriptive methods, process-imitating methods, and structure-simulating methods (Falivene et al. 2007; Koltermann and Gorelick 1996). Each has limitations in its theory and application. The TP/MC geostatistical approach (Carl and Fogg 1996, 1997; Weissmann and Fogg 1999) is used. TP/MC is a structure-simulating method that creates geologically plausible three-dimensional realizations of subsurface heterogeneity, and has been used to model geological heterogeneity (Engdahl et al. 2010; Fogg et al. 2000; Sun et al. 2008; Weismann and Fogg 1999). One advantage of TP/MC is its ability to incorporate quantitative geological information such as facies proportions, mean thicknesses or lengths, and juxtapositioning frequencies. In stochastic hydrogeology, Gaussian-based stochastic approaches (kriging, sequential Gaussian simulation, truncated Gaussian simulation) are widely used to describe spatially heterogeneous hydraulic conductivity. The approach, based on a Markov chain, rather than Gaussian probability model, describes the aquifer heterogeneity in terms of the major hydrostratigraphic facies (hydrofacies), and do not require extensive knowledge of the aquifer hydraulic conductivity distribution. A number of studies have demonstrated that special attention must be paid to the representation of connected features, and that Gaussian-based stochastic

approaches can be insufficient for capturing and generating appropriate connectivity in the high hydraulic conductivity values (Fogg et al. 2000; Gómez-Hernández and Wen 1998; Zinn and Harvey 2003). In some articles, it has been shown that the TP/MC method represents the subsurface architecture of an aquifer and characterizes hydrofacies connectivity better than some conventional geostatistical methods (Lee et al. 2007; Maji et al. 2006; Ye and Khaleel 2008).

A highly resolved model of the heterogeneity in the geological formation of the Seversk area is generated. To capture the essential features of heterogeneity, lithological data from 295 wells spaced irregularly within an area of approximately 4 × 4 km are processed (Fig. 3). This dataset includes lithological logs for about 46 vertical kilometers (at a resolution of 0.5 m), obtained from characterization, monitoring, and injection wells drilled over the past forty years. Core descriptions are categorized as sand, sandy clay, clay sand, and clay. The lithological data are used to develop an indicator database representing the presence or absence of these hydrofacies at each observation point. The mean thickness of all hydrofacies obeys an exponential distribution. The volumetric proportion and mean length of the hydrofacies are estimated from the indicator data using Transition Probability Geostatistics software (T-PROGS) (Carl 1998) (Table 1). T-PROGS uses transition probabilities between hydrofacies that are modeled by Markov chains. The analysis indicates that the horizontal mean length of hydrofacies exceeds the vertical scale by a factor of over 30 (Table 1). Variograms and transition probabilities computed along the azimuths suggest that the effective ranges and mean lengths in the horizontal plane have no directional tendency. Variograms were estimated from the indicator data using Geostatistical Software Library (GSLIB) (Deutsch and Journel 1992). The hydrofacies units serve as the basis for defining the system-scale heterogeneity of an aquifer's hydraulic properties, which enables lithologic descriptions of cores obtained from vertical boreholes to serve as conditioning data for the geostatistical simulations. Based on our analysis of conductivity values, the following hydrofacies are used in the modeling: least permeable (k = 0.0001 m/d [meters per day], clay), poorly permeable (k = 0.001 m/d, sandy clay), permeable (k = 0.03 m/d, clay sand), and most permeable (k = 1 m/d, sand).

Geostatistical simulations were conducted using T-PROGS. The model parameters (hydrofacies proportions, mean lengths, and juxtapositional preferences) were inferred from available quantitative data,

and model realizations were generated and conditioned to these data. Geostatistical parameters were estimated from direct transition probability measurements taken from well logs (Fig. 4, Table 1). Figure 4 shows that the fitted Markov chain model matches the experimental transition probability reasonably well for all hydrofacies. Ten equally probable geostatistical formations with dimensions of 4,300 m × 3,500 m × 130 m were generated (Fig. 5 shows one example). For further analysis, only these ten realizations were considered. Because of the dense network of wells used to condition the models, the difference between realizations was not significant. Each cell measures 25 m × 25 m × 0.5 m, resulting in a total of about 6,260,800 nodes. These grid and domain sizes were used in the groundwater flow and solute transport simulations. In this study, absolute elevation intervals from −100 to −230 m were used. According to the hydrogeological stratification adopted at this site, this covers aquifer III and semipermeable layer D (Rybalchenko et al. 1998). The simulated domain length in each direction is several times larger than the mean lengths (or correlation lengths) of the hydrofacies in this direction. The block size was chosen to be less than the mean hydrofacies lengths in the horizontal and vertical directions, but large enough to satisfy the computational limitations of groundwater flow modeling. The average vertical hydrofacies distributions given by well data and the simulation are compared to validate the simulation results (Fig. 6). Sandy clay hydrofacies has low mean volumetric fraction (Table 1) and its variability in vertical section is not significant, therefore the hydrofacies is not shown in Fig. 6. This Fig. indicates the generally good agreement between the simulated and measured hydrofacies fraction within the studied domain.

In recent years, a number of connectivity indicators have been introduced for the characterization of facies connectivity (Knudby and Carrera 2005). These indicators can be helpful for comparing specific results obtained for different sites by different teams. Hence, the connectivity of the simulated formation in the vertical and horizontal directions was examined. Several connectivity indicators were calculated from the numerical results (Tables 2, 4). The flow connectivity indicator CF_1 (exponent for "power-averaging") was obtained from (Knudby and Carrera 2005)

$$k_{eff} = \left(\frac{1}{V}\int_V k(x)^{CF_1} dV\right)^{\frac{1}{CF_1}}, \quad (1)$$

where V is the domain volume. If $CF_1 = -1$, then a layered medium with flow is perpendicular to the layers. If $CF_1 = 1$, then the flow runs parallel to the layers. CF_2 is defined as the ratio of k_{eff} to k_G, where k_G is the geometric mean of the k-values (Knudby and Carrera 2005). The flow connectivity indicators in the horizontal direction are much greater than those in the vertical direction, which means that the medium has a greater degree of flow channeling (the extent to which a small fraction of the medium provides a large fraction of flux) in the horizontal direction. Transport and flow connectivity indicators for the geological formation under consideration are given in Table 2.

4 Estimation of Effective Hydraulic and Macrodispersion Parameters

4.1 Set-up of Flow and Transport Simulations and Effective Parameter Estimation Methods

Hydraulic conductivity (K) was assigned to each cell based on the simulated hydrofacies determined by the geostatistical realization. Values of K for each hydrofacies were estimated using values in the literature, empirical formulations based on grain-size distributions of sediment samples, field hydraulic tests, and aquifer model calibrations.

To develop long-term predictive models with simplified heterogeneities, the effective hydraulic and macrodispersion properties of the modeled medium were studied. Flow and transport were simulated for heterogeneous realizations. Porosity was assumed to be spatially homogeneous, with a value of 0.2. Transition probabilities in the horizontal plane were assumed to be isotropic. Two simulation runs with different mean flow directions (horizontal/vertical) were performed. The first simulation considered natural groundwater flow from injection site to discharge zone. In the second case, upward flow within the discharge zone was simulated. Constant head boundaries were set on opposite sides of the domain, with no-flow boundaries on all other sides (Fig. 7). Steady-state flow simulations were conducted for each realization with the finite difference code MODFLOW-2000-2005 (Harbaugh et al. 2000). The head difference at opposite boundaries for horizontal and vertical flows was selected to reproduce the typical natural lateral and vertical mean flow gradient for the given environment (Shestakov et al. 2002). The

velocity field was then used in a particle tracking transport code that simulated the three-dimensional solute advective transport by portioning the solute mass into a large number of representative particles (Fig. 7). Particle tracking simulations were performed using PMPATH (Chiang and Kinzelbach 2001), with 4,500 particles in the horizontal and vertical directions. The particles were placed in highly permeable cells, where hydraulic conductivity is greater than 0.001 m/d.

Effective (equivalent) upscaled hydraulic conductivity k_{eff} was determined from steady-state groundwater flow simulations as

$$k_{eff} = \frac{Q\, l}{\omega(H_1 - H_2)}, \tag{2}$$

where Q [m^3/d] is the total flow rate, l [m] is the length of the domain (along primary direction of flow), H_1 and H_2 [m] are the constant heads, and ω [m^2] is the cross-sectional flow area.

The observed breakthrough curves (BTCs) of flux concentration were evaluated as computed from particle arrival time distributions at the control plane. Numerical results can be compared with analytical solutions of the convection-dispersion equation (Fig. 8) for a narrow pulse input of conservative solute under steady-state water flow (one-dimensional transport) (Jury and Roth, 1990)

$$C^f(x,t) = f^f(x,t) = \frac{x}{2\sqrt{\pi D t^3}} exp\left(-\frac{(x-Ut)^2}{4Dt}\right), \tag{3}$$

where C^f is the flux concentration and $f^f(x,t)$ is the probably density function of the arrival time.

Simulations show that the transport of conservative tracer in geological formations is generally non-Fickian, because the BTCs exhibit heavy tails that deviate from the Gaussian plume (Fig. 8). Non-Gaussian features of BTCs obtained at the control planes based on their skewness were also evaluated (Table 2). Note that the BTC shape for horizontal flow is less accurately described by the analytical solution of the macrodispersion equations than for vertical flow.

Despite this non-Fickian behavior in the BTCs, the parameters of the convection-dispersion equation can be estimated for vertical and horizontal transport. Using the temporal moments of BTCs, the mean seepage velocity U and effective longitudinal macrodispersion D for conservative tracers were calculated according to (Jury and Roth 1990; Yu et al. 1999)

$$\mathrm{U} = \frac{x}{M_1}, \tag{4}$$

$$D = \frac{(M_2 - M_1^2)U^3}{2x}, \quad (5)$$

$$M_n = \frac{\int_0^\infty t^n C(x,t)dt}{\int_0^\infty C(x,t)dt}, \quad (6)$$

where x is the distance between the plane of initial particle positions and the control plane of particle sampling, M_1 and M_2 are the first- and second-order normalized moments, $C(x,t)$ is the flux concentration, and t is time. The apparent longitudinal macrodispersivity α_L, apparent porosity n_{eff}, and mean flow velocity V were calculated as

$$\alpha_L = \frac{D}{U}, \quad (7)$$

$$n_{eff} = \frac{V}{U}, \quad (8)$$

$$V = k_{eff} \times I = \frac{Q}{\omega}, \quad (9)$$

where I [-] is the gradient.

4.2 Results of Effective Parameter Estimation

The results indicate that vertical effective conductivity is two orders of magnitude less than horizontal effective hydraulic conductivity (Table 2). This phenomenon relates to the anisotropy of heterogeneity correlation scales.

Our analysis shows that the estimated effective longitudinal macrodispersivity in the vertical direction is one order of magnitude less than that in the horizontal direction (Table 2). These results confirm that longitudinal macrodispersivity is very strongly dependent on flow direction relative to bedding (Engdahl and Weissmann 2010). These dispersivity estimates (Table 2) can ultimately be used as input parameters in transport models that solve the advection-dispersion equation. The apparent parameters calculated in Eqs. (2), (5), and (7) can be viewed as equivalent values in homogeneous porous media that, with the classic convection-dispersion equation, lead to the same spatial moments of the plume as observed in the simulations for heterogeneous porous media. The longitudinal macrodispersivity value in the horizontal direction was used for long-term, regional-scale simulations of natural groundwater flow from the

injection site to the discharge zone, whereas the value in the vertical direction was used to model the flow within the discharge zone (Glinskii et al. 2014).

The apparent porosity for vertical flow of 0.49 is more than double the porosity (0.2) (Table 2). This is because the effective size of vertical heterogeneity (which leads to spatial fluctuations in flow within permeable bodies) is proportional to the horizontal size of clay bodies. Consequently, the flow path in the vertical direction is more convoluted than that in the horizontal direction: the actual path length taken by particles in vertical flow is twice the linear distance between the beginning and end points of the travel path. For horizontal flow, the apparent porosity is just 0.14, because solute transport occurs along the direction of the major bedding planes.

4.3 Analysis of the Number of Simulated Hydrofacies

According to Table 1, the combined volumetric proportion of the most and least permeable facies is 82%. Thus, a binary (permeable-low permeable) system could be considered as a simplified model of heterogeneity. To investigate the influence of the number of facies on the effective parameters, a simulation for two hydrofacies (sand and clay) (Table 3) was generated and the results with the four hydrofacies case described in Sect. 3 were compared. In this two-hydrofacies model, sandy clay was subsumed into the clay hydrofacies, and clay sand was included as sand hydrofacies.

Figure 9 and Table 4 show the results of this additional experiment for vertical and horizontal flow and transport. For the vertical flow, BTCs for both models are approximately the same (Fig. 9(a)). However, significant differences in the BTC shape can be observed in the horizontal direction between the two- and four-hydrofacies models (Fig. 9(b)). This demonstrates the importance of using an appropriate number of facies in heterogeneous models. Effective hydraulic conductivity in the two-hydrofacies model exceeds that in the four-hydrofacies model by a factor of 1.5 in both horizontal and vertical directions (Tables 2, 4). In the horizontal direction, effective longitudinal macrodispersion in the two-hydrofacies model is more than twice that in the four-hydrofacies case. In the vertical direction, this macrodispersion in the two hydrofacies model is 17% greater than when all four hydrofacies are included (Tables 2, 4).

The sensitivity of solute transport behavior to the number of hydrofacies can be explained from a connectivity perspective. A larger proportion and mean horizontal length of sand facies for the two-hydrofacies model (Tables 1, 3) yield a greater degree of connectivity of coarse grained sediments (sand) in the horizontal direction.

5 Upscaling of Hydraulic Conductivity for Coarse Grid

A typical problem in flow and transport simulations is the upscaling of point-scale aquifer properties to coarse numerical grids. The modeling process includes the development of a geological model of heterogeneity using a grid with a comparable frequency to the aquifer characterization data, and this model must be upscaled to a numerical simulation of flow in a heterogeneous medium. In the vertical direction, along-well logs are used to construct the geological model of heterogeneity. The typical resolution of such logs is tens of centimeters. In our study, for example, a resolution of 50 cm was used. To simulate formations of several hundred meters in thickness requires a numerical grid with hundreds or even thousands of nodes in a vertical section. Without the aid of supercomputers, such power grids pose a technical limitation when solving inverse problems or multiple variant simulations. Therefore, methods of upscaling hydraulic conductivity have been the subject of extensive research (Dagan and Indelman 1993; Desbarats and Bashu 1994; Indelman 1993; Li et al. 2011; Pozdniakov and Tsang 1999; Renard et al. 2000; Renard and Marsily 1997). For example, upscaling the conductivity power-averaging formula of Eq. (1) with an exponent parameter $CF_1 = 1/3$ for an infinite volume of integration can be performed for a three-dimensional isotropic medium according to the Landau–Lifshitz–Matheron Conjecture (Renard et al. 2000), or more generally $CF_1 = 1-2n^{-1}$ (Desbarats 1992), where n is the physical dimension of flow. For an anisotropic, perfectly layered system, this exponent is different along the layering ($CF_1 = 1$) and perpendicular to the layering ($CF_1 = -1$). For an anisotropic exponential correlation field of $\log(K)$, with a horizontal to vertical correlation scales ratio ρ ($\rho > 1$), Desbarats and Bashu (1994) proposed the following formula for horizontal averaging

$$CF_1^h = 1 - 2g_{11}. \quad (10)$$

For vertical averaging, this is

$$CF_1^v = 1 - 2g_{33}, \tag{11}$$

where g_{11} and g_{33} are the integrals described by Gelhar and Axness from an anisotropic spectrum corresponding to the exponential autocorrelation function of log(*K*) (Gelhar, 1993, Eq. 4.1.60)

$$g_{11} = \frac{1}{2}\frac{1}{\rho^2 - 1}\left[\frac{\rho^2}{\left(\rho^2 - 1\right)^{1/2}}\operatorname{arctg}\left(\rho^2 - 1\right)^{1/2} - 1\right],$$

$$g_{33} = \frac{\rho^2}{\rho^2 - 1}\left[1 - \frac{1}{\left(\rho^2 - 1\right)^{1/2}}\operatorname{arctg}\left(\rho^2 - 1\right)^{1/2}\right]. \tag{12}$$

The above approach for estimating power-averaging exponents is valid for unbounded media that is for hydraulic conductivity in block sizes that exceed the conductivity correlation scale. For relatively small block sizes (comparable with the correlation scale), the expected value of averaged conductivity for a continuous field of log(*K*) depends on the ratio of block size length to heterogeneity correlation scale (Indelman, 1993; Pozdniakov and Tsang, 1999); that is, the power-averaging exponent depends on the regridding option. The theory of calculating these exponents for discontinuous conductivity fields has not yet been developed.

To illustrate this dependence of power-averaging exponent on regridding, and to understand how the selection of this exponent affects the simulated water balance, the following numerical experiments were performed. Consider the numerical model developed in the previous Sect. with an initial vertical resolution of 260 grid-blocks. Using the initial fine grid, the vertical flow through the domain was simulated with isotropic hydraulic conductivity values in each block, selected according to the hydrofacies. Next, the vertical direction was regridded to combine 2, 4, 5, 10, …, 260 blocks. The vertical and horizontal conductivities for each new block were calculated using Eq. (1) and different power-averaging exponents. Three simulations were performed. The first set used exponents of a perfectly layered system (i.e., $CF_1^v = -1$ and $CF_1^h = 1$). The second set used values obtained from Table 2 (i.e., $CF_1^v = -0.28$ and $CF_1^h = 0.7$), and the third set calculated exponent values using Eqs. (10) to (12) with an effective anisotropy ratio of $\rho = 36$ ($CF_1^v = -0.916$ and $CF_1^h = 0.957$).

According to the results (Fig. 10), no single method of exponent selection produces suitable results for all regridding ranges. The exponents calculated using the whole domain volume gave the worst results. The perfect layering system produced better results, especially for small (from 2 to 5) grid coarsening. The exponents given by Eqs. (10) to (12) allowed vertical regridding of up to one order of magnitude without affecting the overall vertical flow through the domain.

6 Summary and Conclusions

A three-dimensional high-resolution model of the injection area of a radioactive waste disposal site was developed. The geological realization was constructed using Markov chain geostatistics and conditional simulations in the T-PROGS model. This enabled a numerical estimation of effective hydraulic and dispersion properties for the modeled domain.

The results show approximately equal volume fractions of high- and low-permeability hydrofacies within the studied formation and its anisotropy: the horizontal mean length of hydrofacies exceeds the vertical mean length by a factor of over 30. The effective hydraulic properties and longitudinal macrodispersivity were numerically estimated. An analysis of effective hydraulic properties shows some essential hydraulic anisotropy within the medium: vertical effective conductivity is two orders of magnitude less than that in the horizontal direction. This indicates that anisotropy in the effective correlation scales, which leads to hydraulic anisotropy of the overall system, prevents the vertical migration of injected waste.

For the studied medium, BTCs exhibit longer tails and appear to be non-Fickian. Effective longitudinal macrodispersion was calculated using the temporal moments of the observed BTCs. The obtained vertical effective longitudinal macrodispersivity is much larger than typically used values for the homogeneous semipermeable layer in simulations of advective transport through aquitards. For the heterogeneous medium considered here, the rate of transport and effective longitudinal macrodispersivity depend on the direction of flow relative to the bedding. Numerical transport studies show that the estimated effective longitudinal macrodispersivity in the vertical direction is one order of magnitude less than that in the horizontal direction. This implies that, when using a Fickian framework for dispersion modeling in

regional transport simulations, an anisotropic-media dispersion model should be applied (Voss and Provost 2002) with minimal apparent porosity for the most conservative predictions.

A comparison of the two- and four-hydrofacies models for the study site showed that there were significant differences in the BTC shape and effective longitudinal macrodispersion in the horizontal direction. Our results suggest that long-term forecasts of migration are more accurate when a four-hydrofacies model is employed.

In terms of the vertical regridding of regional flow models, the power-averaging method for block-scale conductivity was examined. Our numerical experiments show that the method developed for a continuous log(K) field (Desbarats and Bashu 1994) can be applied to calculate the exponents of a discontinuous hydraulic conductivity field in an aquifer composed of a limited number of anisotropic hydrofacies, each of which is characterized by a single conductivity value. In addition, this approach can be used on a grid that has been coarsened in vertical direction several times.

Acknowledgment This research was supported by the Russian Foundation for Basic Research (projects 14-05-00409-a).

References

Berkowitz B, Klafter J, Metzler R, Scher H (2002) Physical pictures of transport in heterogeneous media: Advection-dispersion, random-walk, and fractional derivative formulations. Water Resour Res 38(10):1191–1203

Carle SF (1998) T-PROGS: Transition Probability Geostatistical Software. University of California, 76 p.

Carle SF, Fogg GE (1996) Transition probability-based indicator geostatistics. Math Geol 28(4):453–476

Carle SF, Fogg GE (1997) Modeling spatial variability with one- and multi-dimensional Markov chains. Math Geol 2(7):891–918

Chiang WH, Kinzelbach W (2001) 3D-Groundwater modeling with PMWIN. First Edition. Berlin, Heidelberg, New York. 346 p.

Dagan G, Indelman P (1993) Upscaling of permeability of anisotropic formations 2. General structure and small perturbation analysis. Water Resour Res 29(4):923–933

Danilov VV (2010) Mathematical modeling of deep disposal of liquid radioactive waste (for example, the Siberian chemical combine): Ph.D thesis, National Research Nuclear University MEPhI, Russia (in Russian)

De Marsily Gh, Delay F, Goncalves J, Renard Ph, Teles V (2005) Dealing with spatial heterogeneity. Hydrogeol J 13:161–183

Dell'Arciprete D, Vassena C, Baratelli M, Giudici M, Bersezio R, Felletti F (2014) Connectivity and single/dual domain transport models: tests on a point-bar/channel aquifer analogue. Hydrogeol J. doi:10.1007/s10040-014-1105-5

Desbarats AJ, Bachu S (1994) Geostatistical analysis of aquifer heterogeneity from the core scale to the basin-scale – a case-study. Water Resour Res 30(3):673–684

Detbarats AJ (1992) Spatial averaging of hydraulic conductivity in three dimensional heterogeneous porous medium. Math Geol 24(3):249–267

Deutsch C, Journel A (1992) GSLIB: Geostatistical Software Library and Usres Guide. Oxford University Press, New York. 340 p.

Engdahl N, Weissmann G (2010) Anisotropic transport rates in heterogeneous porous media. Water Resour Res 46. doi:10.1029/2009WR007910

Engdahl NB, Vogler ET, Weissmann GS (2010) Evaluation of aquifer heterogeneity effects on river flow loss using a transition probability framework. Water Resour Res 46. doi:10.1029/2009WR0079032010

Falivene O, Cabrera L, Munoz JA, Arbues P, Fernandez O, Saez A (2007) Statistical grid-based facies reconstruction and modeling for sedimentary bodies. Alluvial-palustrine and turbiditic examples. Geologica Acta 5(3):199–230

Feehley CE, Zheng C, Molz FJ (2000) A dual-domain mass transfer approach for modeling solute transport in heterogeneous aquifers: Application to the Macrodispersion Experiment (MADE) site. Water Resour Res 36(9):2501–2515

Fleckenstein JH, Fogg GE (2008) Efficient upscaling of hydraulic conductivity in heterogeneous alluvial aquifers. Hydrogeol J 16:1239–1250

Fogg GE, Carle SF, Green C (2000) Connected-network paradigm for the alluvial aquifer system. In: Zhang D and Winter CL (eds) Theory, Modeling, and Field Investigation in Hydrogeology: A Special Volume in Honor of Shlomo P Neuman's 60th Birthday: Boulder, Colorado. Geological Society of America Special Paper, 348:25–42

Foley MG, Bradley DG, Cole CR, Hanson JP, Hoover KA, Perkins WA, Williams MD (1995) Hydrogeology of West Siberian Basin and Tomsk region. PNL-10585. Pacific Northwest Laboratory. Richland, Washington

Gelhar LW (1993) Stochastic subsurface hydrology. Prentice-Hall. 390p

Glinskii ML, Pozdniakov SP, Chertkov LG, Zubkov AA, Danilov VV, Bakshevskaia VA, Samartsev VN (2014) Regional Flow and Transport Simulation of Liquid Radioactive Waste Disposal at the Siberian Chemical Combine for Long- and Super-Long-Term Postinjection Periods. Radiochemistry 56(6):649–656

Gómez-Hernández JJ, and Wen X-H (1998) To be or not to be multi-Gaussian? A reflection on stochastic hydrogeology. Adv Water Res 21(1):47–61

Harbaugh AW, Banta ER, Hill MC, McDonald MG (2000) MODFLOW-2000, the US Geological Survey modular ground-water model – User guide to modularization concepts and the ground-water flow process. Open-File Report 00-92, U.S. Geological Survey Reston. 130 p.

Indelman P (1993) Upscaling of permeability of anisotropic heterogeneous formations: 3. Applications. Water Resour Res 29(4):935–943

Jury WA, Roth K (1990) Transfer functions and solute movement through soil: theory and applications. Birkhfiuser Verlag Basel, Boston, Berlin. 346 p.

Knudby C, Carrera J (2005) On the relationship between indicators of geostatistical, flow and transport connectivity. Adv in Water Resour 28:405–421

Koltermann CE, Gorelick SM (1996) Heterogeneity in sedimentary deposits: A review of structure-imitating, process-imitating, and descriptive approaches. Water Resour. Res. 32(9):2617–2658

Lee S-Y, Carl SF, Fogg GE (2007) Geologic heterogeneity and a comparison of two geostatistical models: Sequential Gaussian and transition probability-based geostatistical simulation. Adv in Water Resour 30:1914–1932

Li L, Zhou H, and Gómez-Hernández JJ (2011) A comparative study of three-dimensional hydraulic conductivity upscaling at the macro-dispersion experiment (MADE) site, Columbus Air Force Base, Mississippi (USA). J Hydrol 404:278–293

Liu G, Zheng C, Gorelick SM (2004) Limits of applicability of the advection-dispersion model in aquifers containing connected high-conductivity channels. Water Resour Res 40. Doi:10.1029/2003WR002735

Maji R**,** Sudicky EA, Panday S, Teutsch G (2006) Transition Probability/Markov Chain Analysis of DNAPL Source Zone and Plumes. Ground Water 44 (6):853–863

Neuman SP, Tartakovsky DM (2009) Perspective on theories of non-Fickian transport in heterogeneous media. Adv in Water Resour 32:670–680.

Pozdniakov S and Tsang CF (1999) A semianalytical approach to spatial averaging of hydraulic conductivity. J Hydrol 216(1–2):78–98

Pozdniakov SP, Bakshevskaya VA, Krohicheva IA, Danilov VV, Zubkov AA (2012) The Influence of Conceptual Model of Sedimentary Formation Hydraulic Heterogeneity on Contaminant Transport Simulation. Moscow Univ. Geol. Bull. 67(1):43–51

Pozdniakov SP, Bakshevskaya VA, Zubkov AA, Danilov VV, Rybalchenko AI, Tsang C-F (2003) 3D Modeling of Injected Waste Transport in Sandy-Clay Formation, Second International Symposium «Underground Injection Science and Technology», Lawrence Berkeley National Laboratory. Berkeley, California, October 22-25, 51–52

Pozdniakov SP, Bakshevskaya VA, Zubkov AA, Danilov VV, Rybalchenko AI, Tsang C-F (2005) Modeling of Waste Injection in Heterogeneous Sandy-Clay Formation. In: Tsang C-F, Apps JA (eds) Underground Injection Science and Technology. Elsevier, pp 203–219

Renard Ph, De Marsily G (1997) Calculating equivalent permeability: a review. Adv in Water Resour 20(5):253–278

Renard Ph, Loc'h Le, Ledoux E, Marsily G, Mackay R (2000) A fast algorithm for the estimation of the equivalent hydraulic conductivity of heterogeneous media. Water Resour Res 36(12):3567–3580

Ritzi RW (2000) Behavior of indicator variograms and transition probabilities in relation to the variance in lengths of hydrofacies. Water Resour Res 36(11):3375–3381

Rybalchenko AI, Pimenov MK, Kostin PP, Balukova VD, Nosuckhin AV, Mikerin EI, Egorov NN, Kaimin EP, Kosareva IM, Kurochkin VM (1998) Deep injection disposal of liquid radioactive waste in Russia. Edited by Foley MG and Ballou L. Battelle Press, Columbus Richland, Washington. 205p.

Shestakov VM, Kuvaev AA, Lekhov AV, Pozdniakov SP, Rybalchenko AI, Zubkov AV, Davis PA, Kalinina EA (2002) Flow and transport modeling of liquid radioactive waste injection using data from the Siberian Chemical Plant Injection Site. Environ Geol 42(2-3):214–221

Sun AY, Ritzi RW, Sims DW (2008) Characterization and modeling of spatial variability in a complex alluvial aquifer: Implications on solute transport. Water Resour Res 44. doi:10.1029/2007WR006119

Voss CI, Provost AM (2002) SUTRA, a model for saturated-unsaturated variable-density ground-water flow with solute or energy transport, U.S. Geological Survey Water-Resources Investigations Report 02-4231. 291p.

Weissmann GS, Fogg GE (1999) Multi-scale alluvial fan heterogeneity modeled with transition probability geostatistics in a sequence stratigraphic framework. J Hydrol 226:48–65

Ye M and Khaleel R (2008) A Markov chain model for characterizing media heterogeneity and sediment layering structure. Water Resour Res 44. doi:10.1029/2008WR006924

Yu C, Warrick AW, Conklin MH (1999) A moment method for analyzing breakthrough curves of step inputs. Water Resour Res 11:3567–3572

Zhang Y, Benson D, Baeumer B (2007) Predicting the tails of breakthrough curves in regional – scale alluvial systems. Ground Water 45(4):473–484

Zheng C, Gorelick SM (2003) Analysis of solute transport in flow fields influenced by preferential flowpaths at the decimeter scale. Ground Water 41(2):142–155

Zinn B, Harvey CF (2003) When good statistical models of aquifer heterogeneity go bad: A comparison of flow, dispersion, and mass transfer in connected and multivariate Gaussian hydraulic conductivity fields. Water Resour Res 39(3):1051–1068

Table 1 Hydrofacies properties of the geological formation being studied

Hydrofacies category	Mean thickness (m)[a]	Mean length (m)[b]		Proportion (-)
		vertical	horizontal	
Sand	4.99	4.5	243	0.42
Clay sand	4.30	3.8	109	0.15
Sandy clay	3.20	2.7	87	0.03
Clay	5.50	6.1	287	0.40

[a] Mean thickness is computed from borehole records

[b] Mean length is inferred from transition probabilities

Table 2 Estimated parameters for ten three-dimensional high-resolution four-hydrofacies geostatistical realizations

Parameter		Value for the direction of flow					
		vertical			horizontal		
		Min	Max	Mean	Min	Max	Mean
Effective conductivity k_{eff}, m/d		0.0013	0. 0018	0.0015	0.298	0.305	0.302
Effective longitudinal macrodispersion D, m^2/d		0.004	0.007	0.005	0.99	1.09	1.04
Apparent porosity n_{eff}, -		0.45	0.52	0.49	0,13	0,14	0,14
Longitudinal macrodispersivity α_L, m		39	54	43	388	412	402
Transport connectivity indicators	CT_1[a]	6.77	9.94	8.12	1.75	1.84	1.78
	CT_2[b]	1	1.38	1.18	1.18	1.41	1.29
Indicators of flow connectivity	CF_1[c]	-0.3	-0.24	-0.28	0.69	0.71	0.7
	CF_2	0.1	0.14	0.12	23.8	24.4	24.1

[a]$CT_1 = t_{ave}/t_5$, where t_{ave} is the average arrival time, t_5 is the time at which 5% of the solute has arrived at the control plane (Knudby and Carrera 2005)

[b]CT_2 is the coefficient of skewness of arrival time distribution (Knudby and Carrera 2005)

[c] CF_1 – exponent for "power-averaging"

Table 3 Characteristic geological formation depicted as a two-hydrofacies model

Hydrofacies category	Mean thickness (m)	Mean length (m)[a]		Horizontal mean length (m)[b]	Proportion (-)
		vertical	horizontal		
Sand (contents sand and clay sand from four-hydrofacies model)	4.79	9.4	497	409	0.58
Clay (contents clay and sandy clay from four-hydrofacies model)	5.23	6.8	360	309	0.42

[a] Mean length is inferred from transition probabilities

[b] The horizontal mean length was calculated as $L_k = a_k/3(1 - p_k)$ where a_k is effective range is computed from variograms (exponential model), p_k is proportion of hydrofacies (Ritzi 2000)

Table 4 Estimated parameters for binary three-dimensional high-resolution geostatistical realization

Parameter		Value for the direction of flow	
		vertical	horizontal
Effective conductivity k_{eff}, m/d		0.0024	0.45
Effective longitudinal macrodispersion D, m^2/d		0.006	2.31
Apparent porosity n_{eff}, -		0.80	0.14
Longitudinal macrodispersivity α_L, m		52.1	616.5
Transport connectivity indicators	CT_1	14.66	1.47
	CT_2	1.13	2.50
Indicators of flow connectivity	CF_1	-0.22	0.69
	CF_2	0.12	22.1

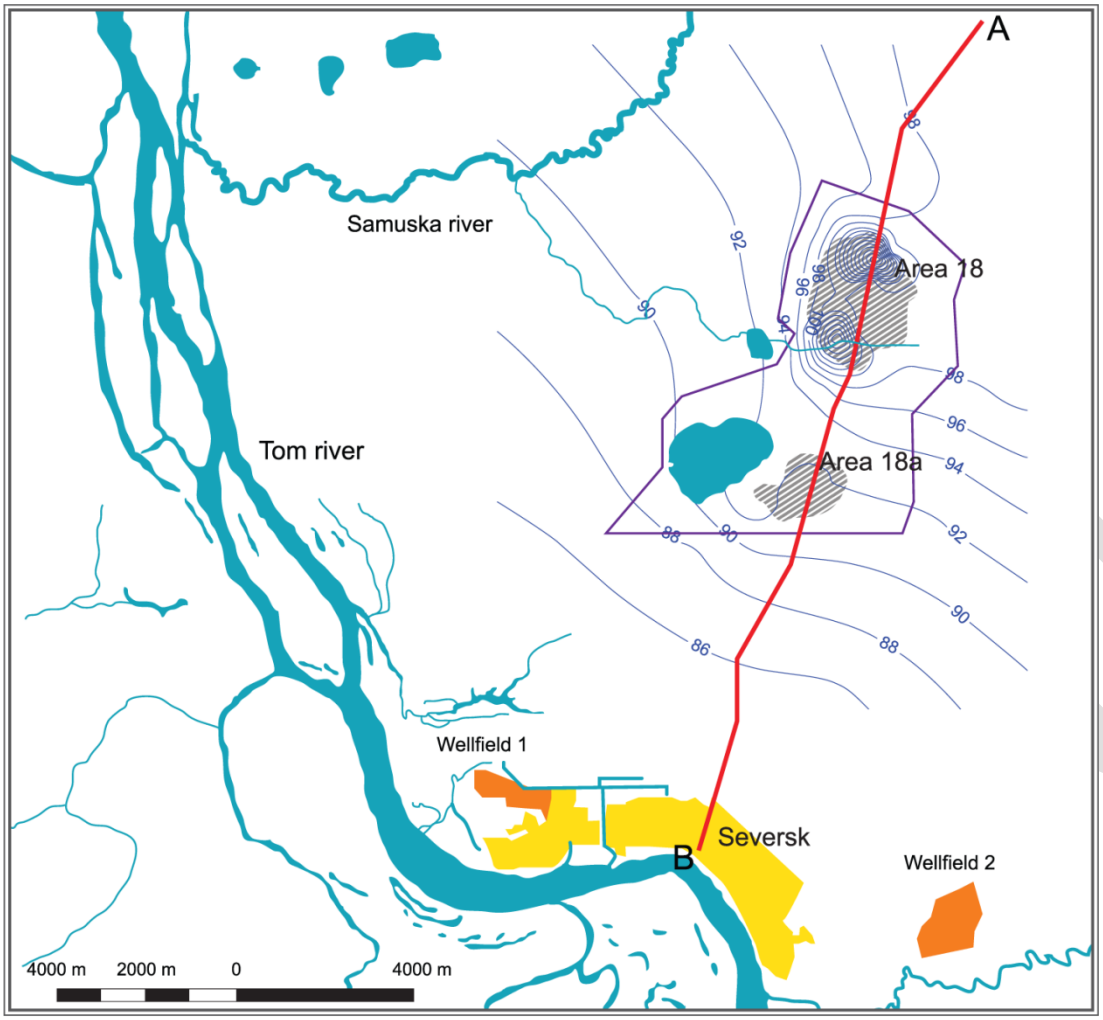

Fig. 1 Location of the site being studied

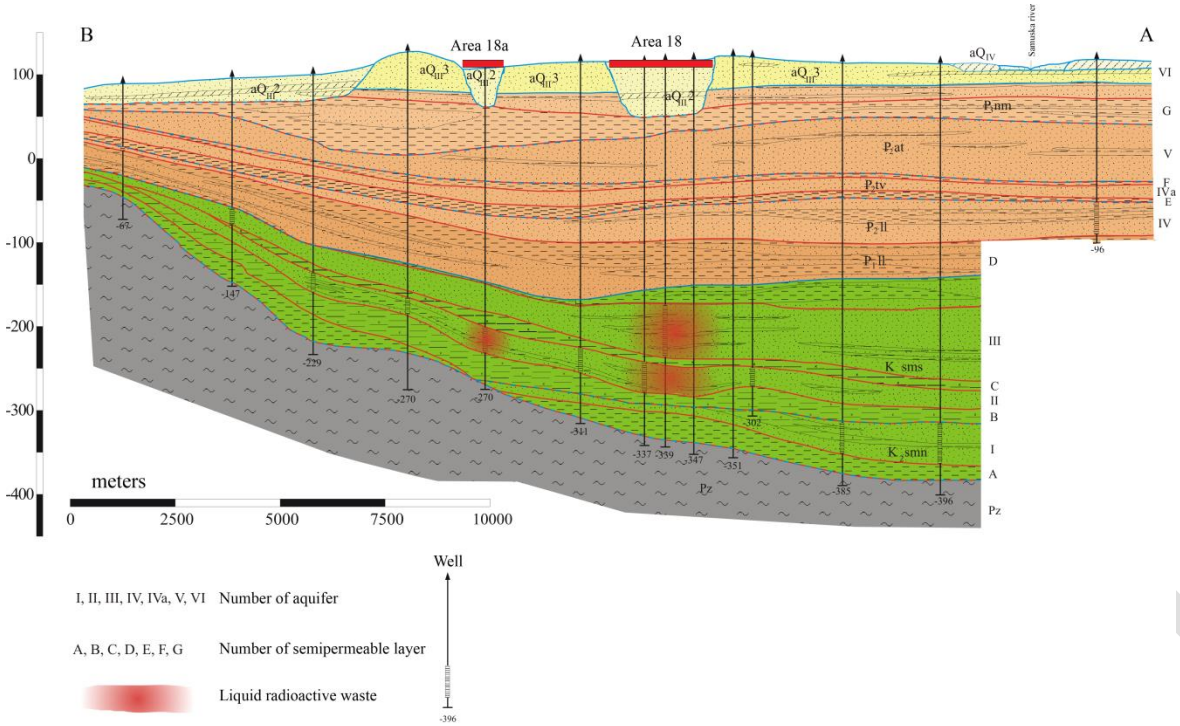

Fig. 2 Geological cross-section of the injection site (taken from Danilov (2010) and modified by the authors)

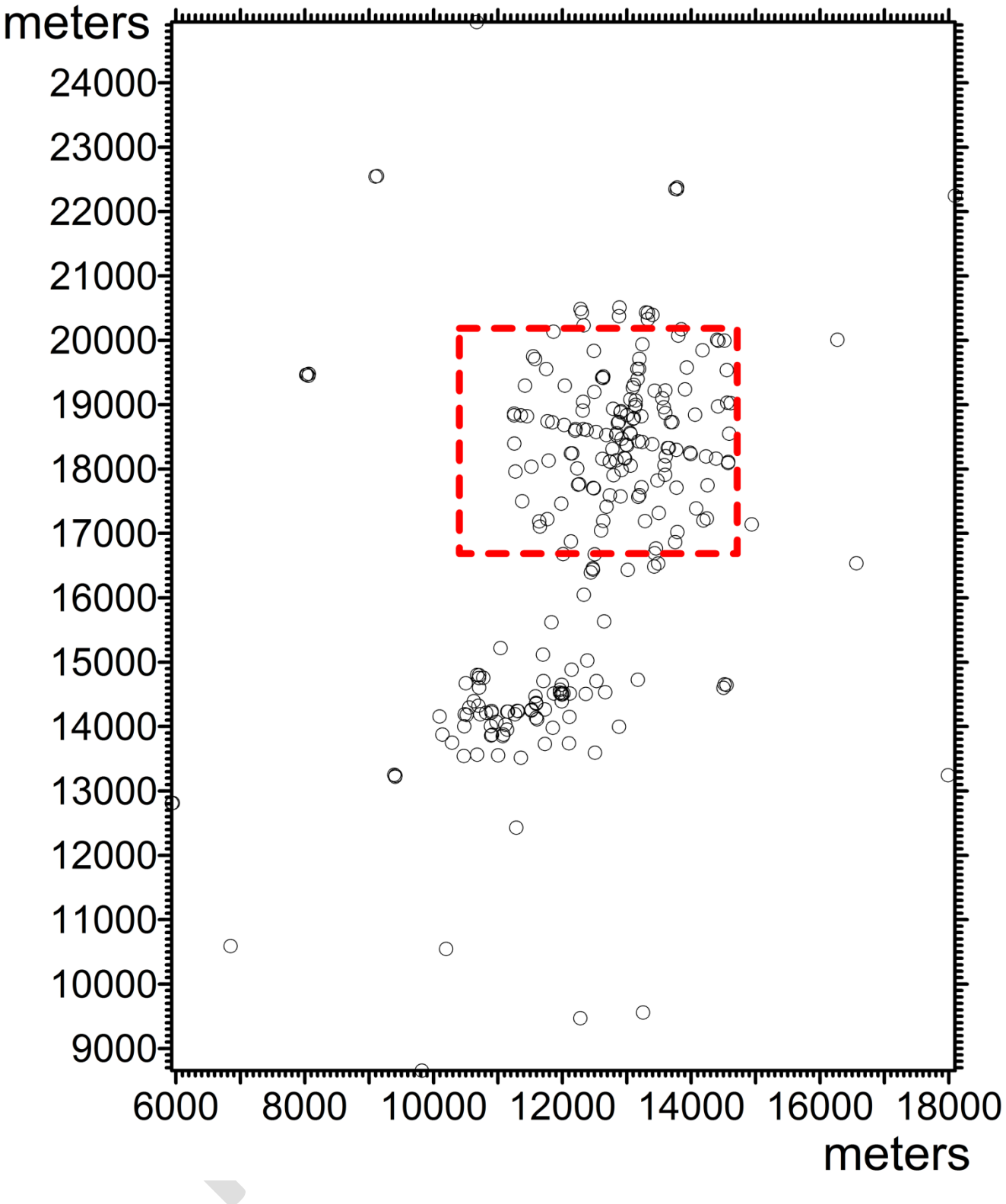

Fig. 3 Location of 295 wells with lithological logs. The dashed line shows the area of the model

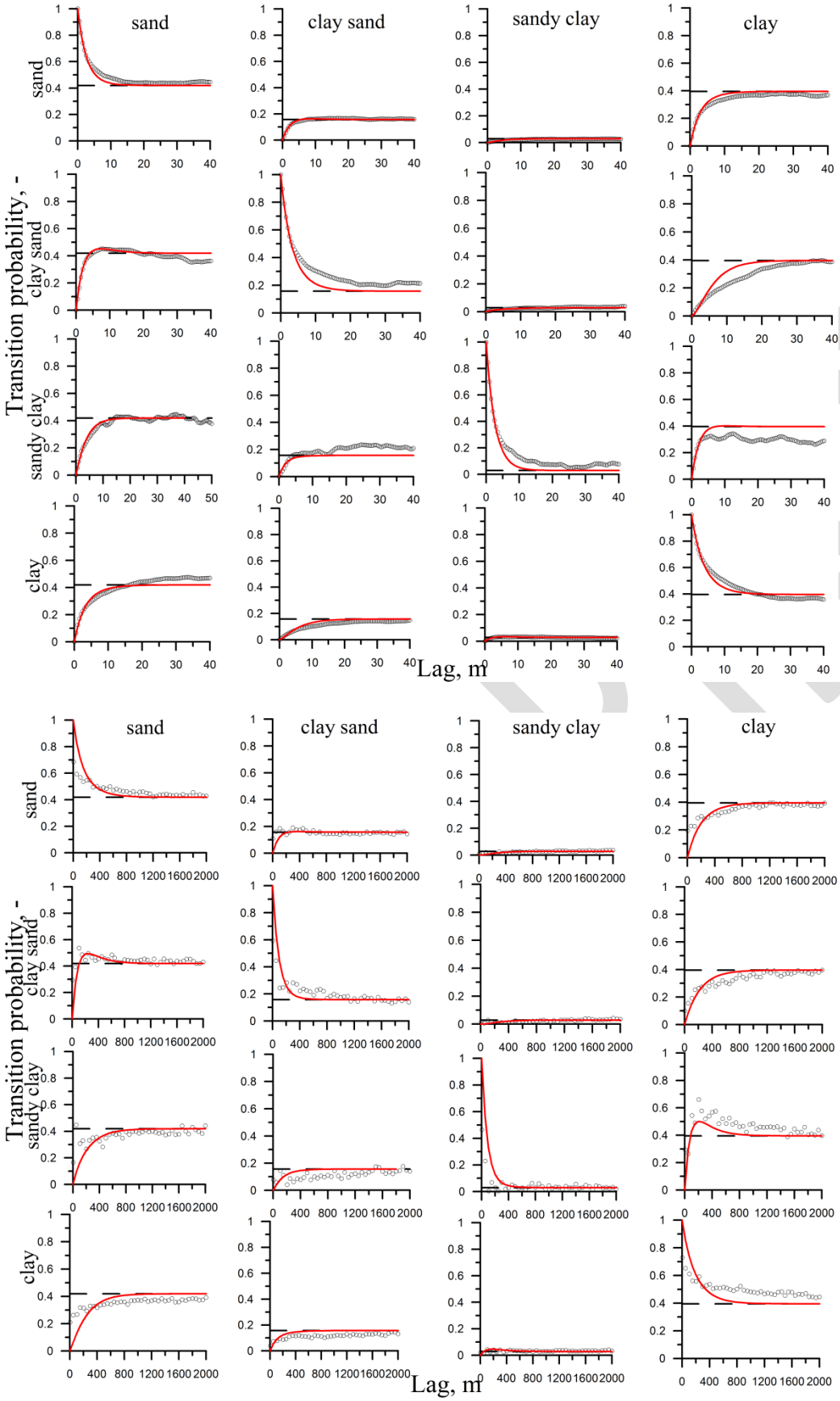

Fig. 4 Transition probability matrix in vertical (a), and horizontal (b) directions: core data measurements (dots), Markov chain model (solid line), and proportions (dashed line)

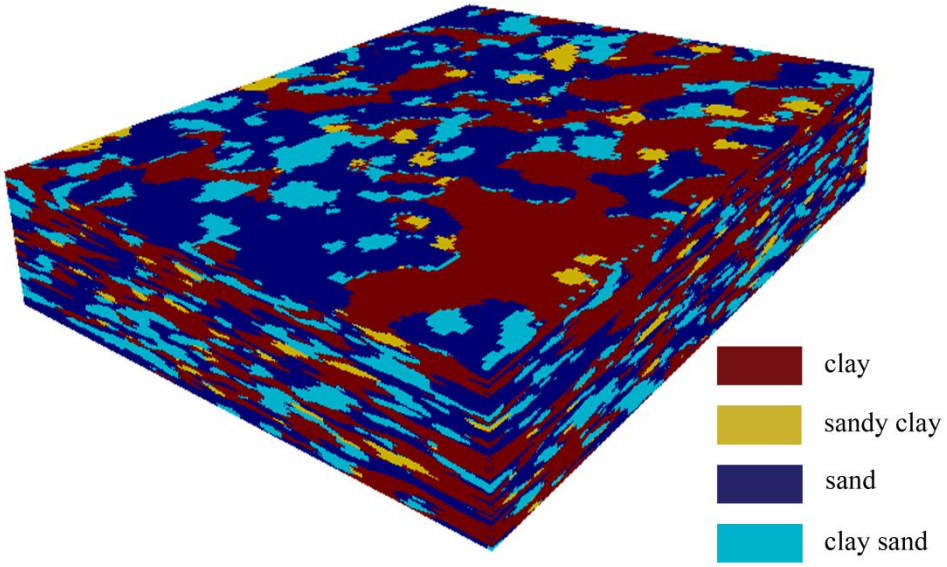

Fig. 5 Three-dimensional view of the heterogeneous model for realization 1

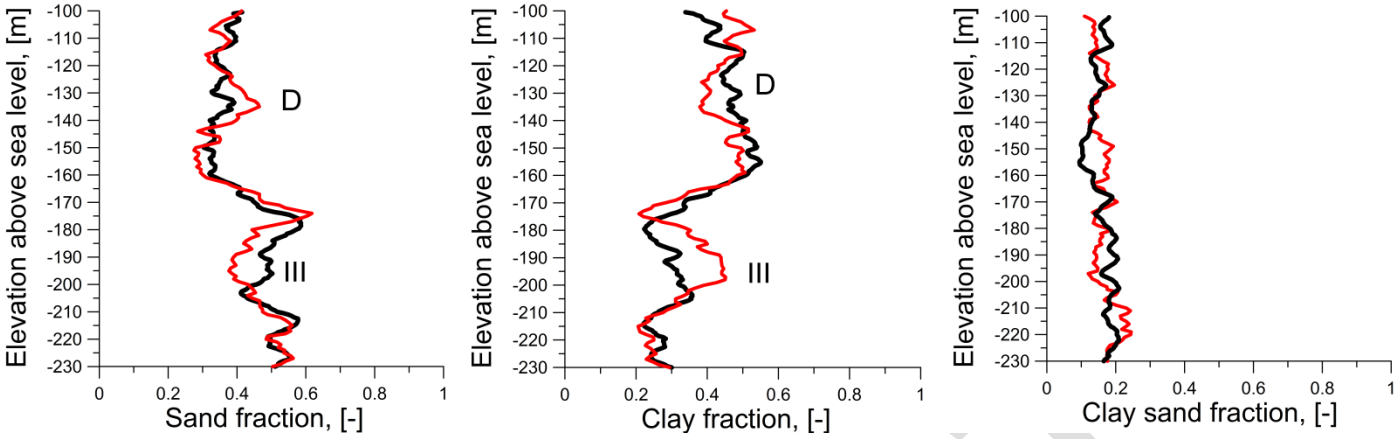

Fig. 6 Averaged distribution of volumetric fraction of hydrofacies in vertical section: simulated (black line) and measured over all wells (empirical data) (red line)

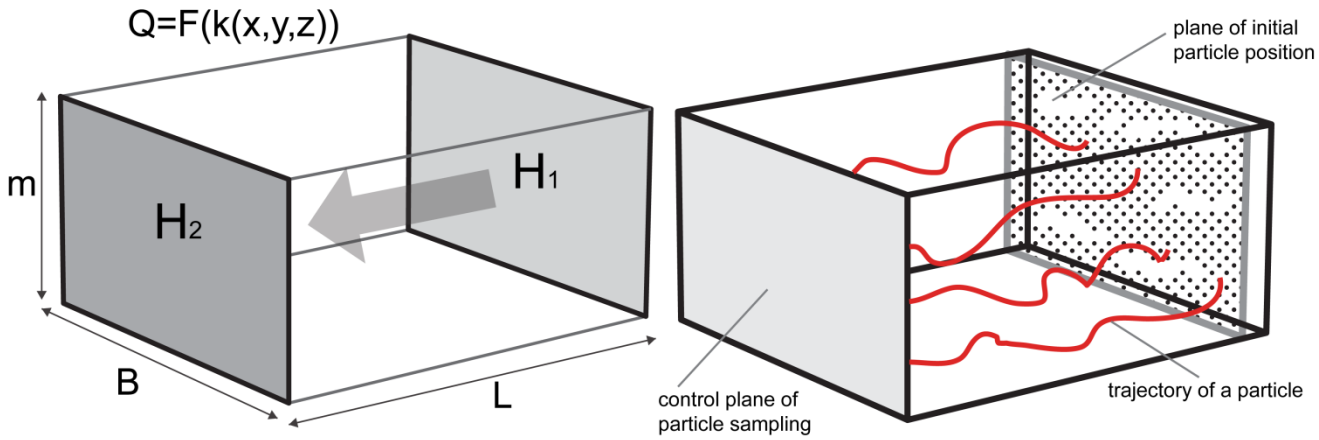

Fig. 7 Set-up of flow and transport simulations. Flow and transport problem is rotated 90° to investigate flow and transport in vertical direction

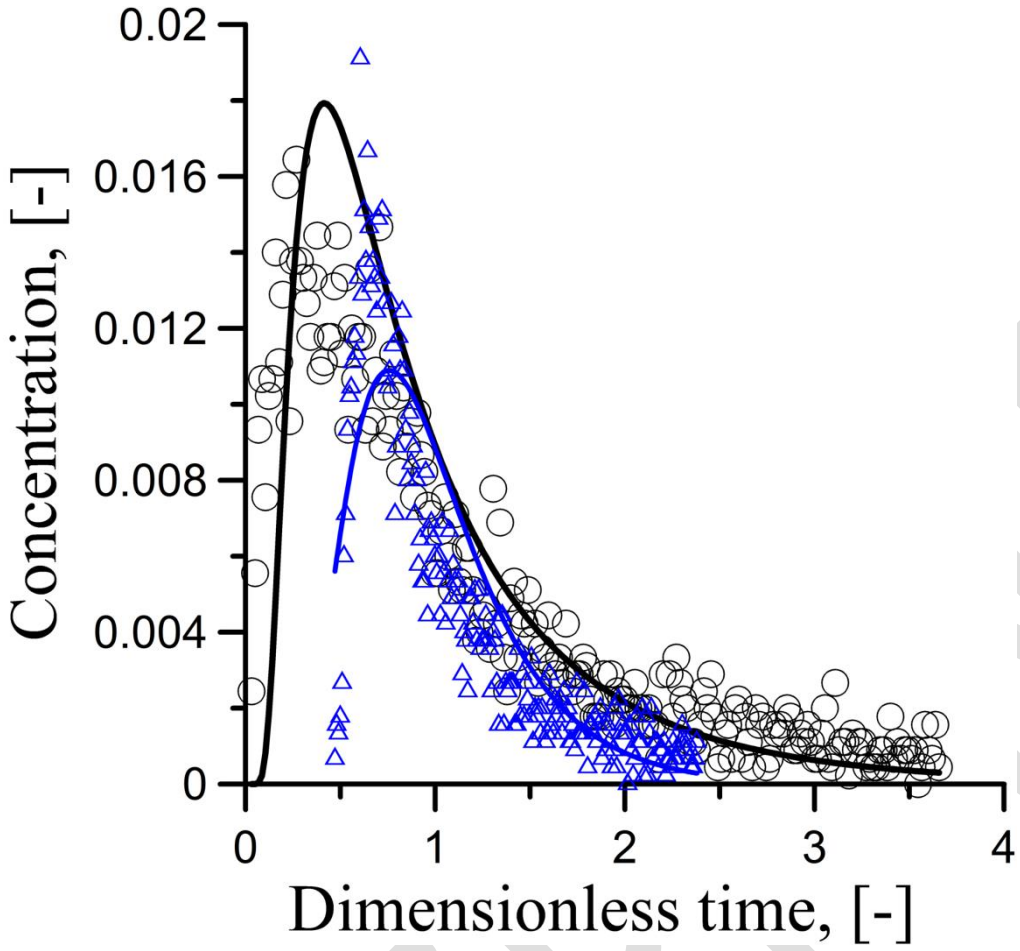

Fig. 8 Breakthrough curves (symbols) and analytical solutions of the convection-dispersion equation (solid line) in horizontal (blue line) and vertical (black line) directions for realization 1. Normalized time is calculated as $\tau = \frac{t \times V}{l \times n}$, where t is particle arrival time, n is porosity

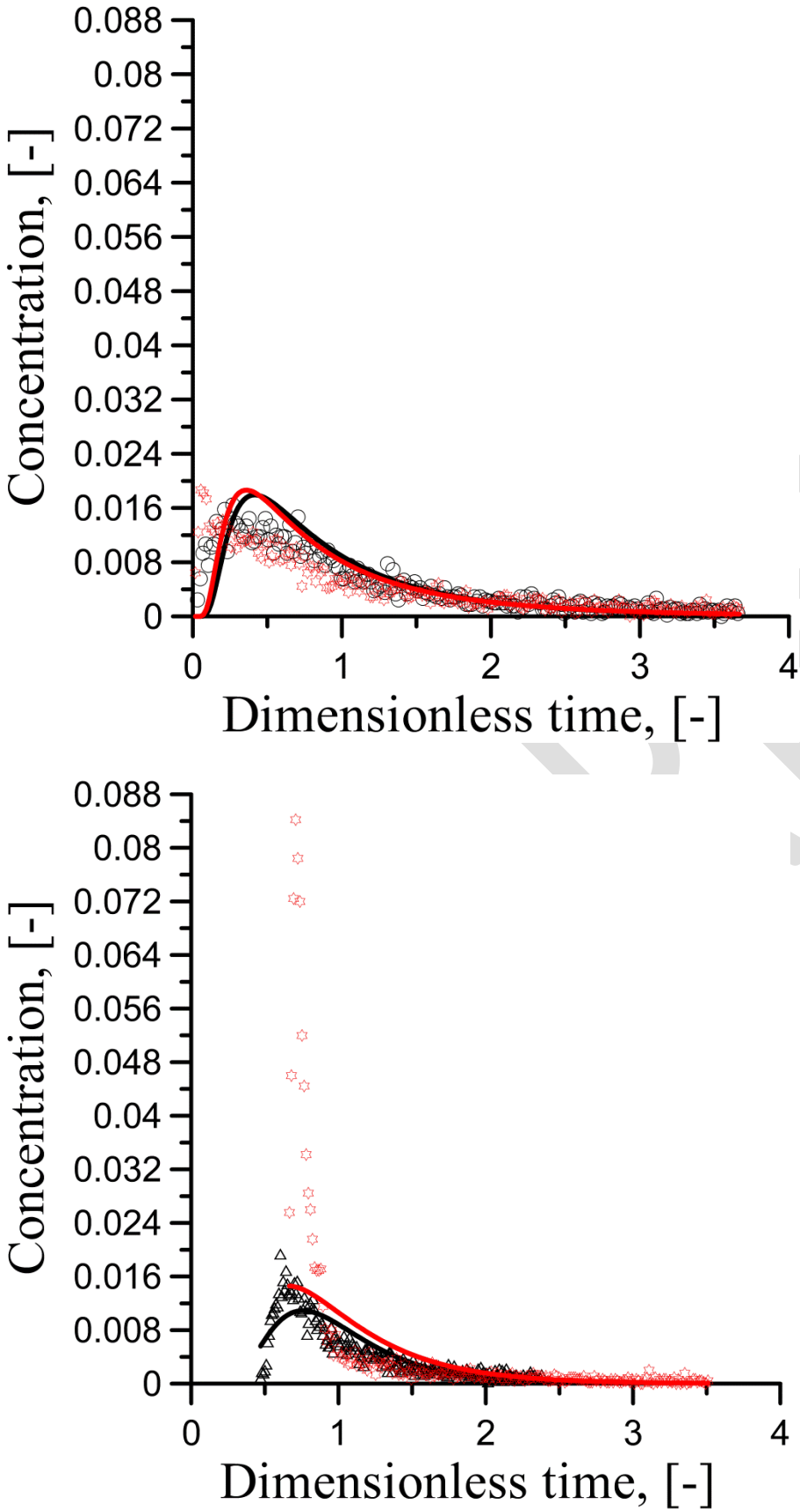

Fig. 9 Breakthrough curves (symbols) and analytical solutions of the convection-dispersion equation (lines) in vertical (a), and horizontal (b) directions for two-hydrofacies (red symbol and line) and four-hydrofacies (black symbol and line) medium

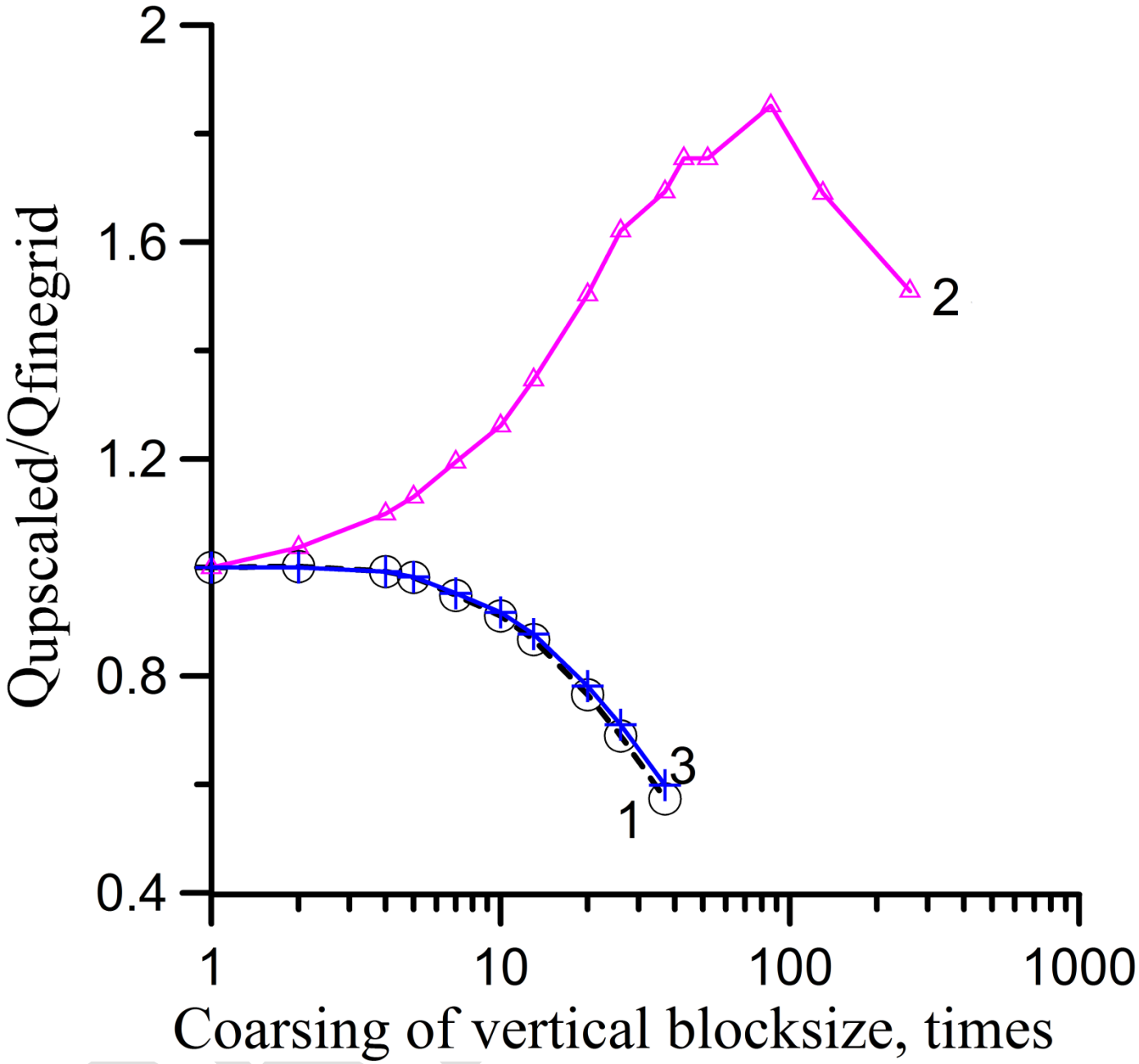

Fig. 10 Ratio of vertical flow through domain obtained on coarse vertical grid to flow obtained on fine vertical grid. Curves labeled by different values of scaling exponent CF_1: 1 – Arithmetic mean for horizontal conductivity and harmonic mean for vertical conductivity, 2 – Values of −0.28 for vertical conductivity and 0.7 for horizontal conductivity (Table 2), 3 – Values calculated using Eq. (1) and Eqs. (10) to (12)